Journal of Wind Engineering & Industrial Aerodynamics 170 (2017) 68–80

Contents lists available at ScienceDirect

Journal of Wind Engineering & Industrial Aerodynamics

journal homepage: www.elsevier.com/locate/jweia

Assessment of various turbulence models (ELES, SAS, URANS and RANS) for predicting the aerodynamics of freight train container wagons

Siavash Maleki [a,*], David Burton [a], Mark C. Thompson [a]

[a] Fluids Laboratory for Aeronautical and Industrial Research (FLAIR), Department of Mechanical and Aerospace Engineering, PO Box 31, Monash University, 3800, Australia

ARTICLE INFO

Keywords:
Embedded large eddy simulation (ELES)
Scale-adaptive simulation (SAS)
Unsteady Reynolds-averaged Navier-Stokes equations (URANS)
Reynolds-averaged Navier-Stokes equations (RANS)
Hybrid RANS/LES
Freight train aerodynamics

ABSTRACT

This study presents an assessment of the capabilities of various turbulence modelling approaches —ELES, SAS, URANS and RANS—to predict the aerodynamic flow around a double-stacked freight wagon, both in isolation and within a train. The numerical predictions are compared with experimental measurements at the same Reynolds number to determine the accuracy of each model. Specifically, aerodynamic drag, front and rear surface pressures, planar velocity fields and skin friction lines are validated against the wind tunnel results. In particular, predictions from the ELES and SAS models show good agreement with the wind tunnel data, both qualitatively and quantitatively. Indeed, ELES predicts both the range and distribution of the rear-face surface pressure very closely, indicating that the separated flow is also likely to be well predicted. Both SAS and ELES predict the pressure drag of the multi-wagon configuration to within 2% of the experimental value. However, the steady RANS model predicts the trends in pressure drag in line with the experiments as the front and rear gaps are varied, even though individual drag predictions are considerably worse. Overall, the set of results establishes the benefits and deficiencies of using particular turbulence models to capture different aspects of freight train aerodynamics.

1. Introduction

Aerodynamic characteristics of intermodal freight trains are highly complex and influenced by a variety of parameters. The extreme length (up to 2 km), and bluffness and irregularity of the containers, have a significant impact on the overall aerodynamic drag. Even though the typical operational speed of a freight train is much lower than that of high-speed passenger trains, at 115 km h^{-1} 80% of total drag is still due to aerodynamic drag (Li et al., 2017).

Intermodal freight trains are designed to carry shipping containers. In contrast with passenger trains, which mostly have identical carriage geometries, intermodal freight trains often have wagons of various sizes, known as *flatcars*, *well-cars* and *skeletonised cars*. As a result of the varying geometry and loading patterns of each train, the aerodynamic performance of each train can vary significantly. Furthermore, as containers are loaded and unloaded at intermediate hubs the loading configuration of the train changes (Li et al., 2017).

Apart from their loading configuration and varying geometry, the length of intermodal freight train can reach up to ~ 2 km with a length-to-height ratio of $L/H = 250$. This ratio is 2.5 times higher than the length-to-height ratio of a high-speed train. Investigation of a bluff body with such an extreme length numerically has always been challenging. It is extremely computationally expensive to simulate an entire train.

Watkins et al. (O'Rourke et al., 1990) conducted wind tunnel testing of 1:10 scale wagons to determine the minimal model configuration for simulating a single wagon located within the middle section of a train. His analysis suggested that 1.5 wagons upstream and 0.5 wagons downstream are required to simulate a wagon, when not affected by the locomotive or the end of the train. Golovanevskiy et al. (2012) conducted a numerical analysis to study the influence of the locomotive and the last wagon on the aerodynamic drag. He found, excluding the three wagons from the front and rear of the train, that all other wagons in a long train experience a similar drag coefficient.

Ahmed et al. (1984), who first proposed using a simplified vehicle to study the main feature or automobile aerodynamics, highlighted the contribution of pressure drag, which accounts from 76% to 85% of the total drag experienced by a vehicle. The pressure drag is the difference between the pressure forces acting on the front and rear surfaces of a body. Ahmed's findings indicate that for a bluff body, drag reduction can mainly occur through reducing the pressure drag, which is generally caused by flow separation and energy losses from rear facing surfaces.

Schito and Braghin (2012) conducted wind tunnel tests and

* Corresponding author.
E-mail address: siavash.maleki@monash.edu (S. Maleki).

http://dx.doi.org/10.1016/j.jweia.2017.07.008
Received 10 April 2017; Received in revised form 14 June 2017; Accepted 14 July 2017
Available online 17 August 2017
0167-6105/© 2017 Published by Elsevier Ltd.

numerical simulations to investigate a platoon of six square-back vehicles. They reported the drag progressively reduced up to the fourth body but reached a constant value for the remaining bodies. Mirzaei and Krajnovic (2016) performed LES simulations to study the flow structures for a long homogenous platoon at four inter-vehicle distances using a similar setup to Schito and Braghin (2012). To reduce the computational cost, they simulated only one *pitch* of domain, where the computational domain starts from the middle of one vehicle to the middle of the next, using periodic streamwise boundary conditions.

Osth and Krajnovic (2014) conducted LES simulations of the aerodynamics of an isolated single-stacked container wagon, and a wagon situated within a train with wagons ahead and behind. Periodic streamwise boundary conditions were employed in the latter case to model the condition of a container at the arbitrary position in the train. The drag coefficient reported for the periodic wagon was 0.09, which is 1/10 th of the value for a single wagon. They showed the existence of two symmetrical counter-rotating vortices in the gaps between two wagons, making the train act almost like one connected body, and consequently causing a significant reduction in drag.

Uystepruyst and Krajnovic (2013) performed LES simulations of the flow around four cuboids aligned in a row, with one forced to undergo in-line oscillation. The models used in the simulations were simple sharp-edged rectangular boxes, representing idealised minivans. This body geometry is similar to the model used in the present study. In-line oscillation was defined as when one of the platoon members was forced to move periodically in a streamwise direction with a specified velocity and displacement amplitude. Time-mean measurements of the drag coefficient of each member of the platoon were undertaken to show the significant effect of tandem configuration on individual drags. The LES study confirmed all bodies experienced a reduction in drag from belonging to a combined configuration. The reported drag reductions for the first, second, third and last models were 15%, 70%, 80% and 60%, respectively.

Soper et al. (2014) conducted scale-model experiments to evaluate the slipstream of a Class 66 container freight train. Various configurations were tested representing different container loading efficiencies. Their findings showed an increase in boundary-layer growth with higher turbulence intensities through lowering container loading efficiencies. Flynn et al. (2014) performed a *Delayed Detached-Eddy Simulation* (DDES) simulation to study the slipstream behaviour of an operational freight train. These simulations were validated against the experiments of Soper et al. (2014), noting that the numerical model had a good degree of similarity to the physical model used in the experimental work. Slipstream velocities along the side and roof of the train were studied. The maximum induced streamwise velocity was reported near the nose due to its relatively sharp corners. In addition, the largest inter-wagon spacing was reported to lead to the largest slipstream velocities in the boundary layer region.

Hemida and Baker (2010) performed an LES study of the unsteady flow around a simplified freight wagon subjected to a cross wind at 90° yaw angle. Spanwise periodicity was employed to simulate the influence of neighbouring wagons. Their results indicated that flow separation at the windward side of the container was responsible for creating a large region of flow separation on the roof of the container. In addition, Flynn et al. (2016) conducted DDES simulations to evaluate the effect of crosswinds with two different yaw angles: 10° and 30°, on the slipstream of a freight train.

Li et al. (2017) created a setup consisting of seven wagons aligned longitudinally in an attempt to understand the impact of the loading configuration on drag, and consequently to estimate the pressure drag of an entire train by the summation of individual wagon drag contributions. They conducted wind tunnel testing in which both the upstream and downstream gaps (G_f, G_b) were varied over 7 sizes, resulting in a combination of 49 upstream and downstream gap spacings. The overall aim was to determine the influence of different upstream and downstream container loading patterns on the pressure drag of a fully loaded test wagon. In line with past literature, they showed the drag of a wagon increases with enlargement of both G_f and G_b. In addition, they reported G_b has very little impact on the upstream pressure distribution due to the length of the wagon. Most importantly, Li et al. (2017) showed the greatest opportunity for drag saving occurs between $G_f = 1.77W$ and $G_f = 3.23W$, where W represents the wagon width. This range is where the highest rate of drag increase was observed. They showed a flow regime change within the gap causes such a high gradient. At increasing gap sizes, the pressure becomes higher and more uniform over the front surface, resulting in a similar distribution to a single wagon in free-stream.

The main objective of this study is to assess the fidelity of the ELES, SAS, URANS and RANS approaches for predicting the aerodynamic drag and flow topology matching the flow setup of wind tunnel experiments conducted by Li et al. (2017). A similar recent comparison study has been undertaken for high-speed train aerodynamics by Wang et al. (2017). Developing an accurate numerical model of a freight train capable of estimating the drag of a train with any loading configuration would be of considerable use. It would allow a near-optimal loading configuration of an entire train to be determined, leading to improved fuel economy and reduced greenhouse emissions. Another advantage of a predictive numerical model is that it would enable the study of detailed flow dynamics, which is much more difficult using a wind tunnel. It will assist in understanding the underlying flow mechanisms responsible for the flow regime change reported by Li et al. (2017) over the G_f gap range $1.77W$ – $3.23W$.

The paper is structured as follows. A description of the freight wagon model is presented in Section 2. The meshing, computational domain and boundary conditions for the single wagon and multiple wagons at $G_f = 9.38W$ and $G_b = 3.23W$ are discussed in Section 3. Amongst all 49 G_f and G_b combinations, most experimental data is available for this gap size combination. The numerical method is presented in Section 4. The sensitivity study as well as a comparison between numerical results and experimental data are presented in Section 5. The paper ends with conclusions in Section 6.

2. The freight-train wagon model

The model used in our numerical simulations is a double-stacked container wagon tested in the Monash University 450KW closed-circuit wind tunnel by Li et al. (2017). The wind tunnel has a test section of $16 \times 2 \times 2$ m^3 ($L \times W \times H$), giving a wind tunnel blockage of 2.4%. The experimental model is a 1/14.6th scale model of 48 ft double-stacked container wagon, with $L = 1000$ mm, $W = 171$ mm and $H = 438$ mm representing a section of a freight train. The ground clearance was $E = 28$ mm, corresponding to the radius of a full-scale 32inch wheel. The spaces between upstream and downstream wagons were filled, in line with the experimental model, to reduce extraneous complexity of the train geometry to focus of the local loading configuration. A full description of the experimental setup can be found in Li et al. (2015, 2017).

The coordinate system adopted in this study is shown in Fig. 1. For convenience, the streamwise position, X, is normalized by the model length (L), with $X = 0$ and 1 corresponding to the positions of the leading and trailing edges of the test wagon, respectively. The cross-stream position, Z, is normalized by the model width (W), and the vertical position, Y, is normalized by model height (H), unless otherwise stated.

3. Computational domain and boundary conditions

In the present work, two numerical models were generated: an isolated double-stacked freight wagon in freestream (case 1), and a multiple wagon setup, consisting three wagons upstream and downstream of the test wagon with gap ratio combination $G_f = 9.38W$ and $G_b = 3.23W$ (case 2). As previously mentioned, this selected gap size combination has the most experimental data available of all cases tested in the wind tunnel

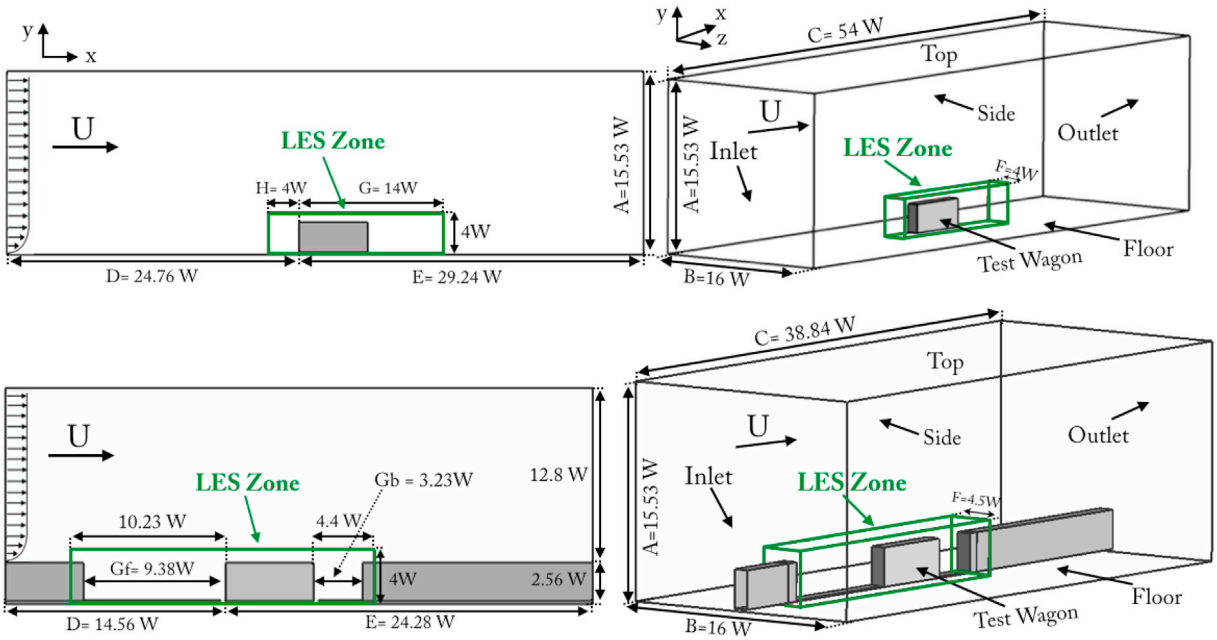

Fig. 1. Top: Geometry of a doubled-stacked single wagon and computational domain for case 1 with LES zone indicated; Bottom: Geometry of multiple double-stacked wagons and computational domain for case 2 with LES zone marked.

experiments. Aspects of the numerical model and the computational domain for cases 1 and 2 are shown in the Fig. 1. All the geometric quantities shown in Fig. 1 were normalised by the body width, W, equal to 0.171 m.

For case 1, a computational domain of height $A = 15.53W$, spanwise width $B = 16W$, and length $C = 54W$ was selected. The blockage area of the selected cross section was 1.03%, slightly lower than for the wind-tunnel study. The position of the front surface of the test wagon to the inlet was $D = 24.76W$, equivalent to the position of test wagon relative to the leading edge of a splitter plate in the wind-tunnel experiment. The simulated boundary layer profile at inlet had a boundary layer thickness of $\delta = 0.46H$ for a 30 ms^{-1} free-stream velocity. This is equivalent to the flow profile measured at the leading edge of the splitter plate using a cobra probe[1] This flow velocity corresponds to a Reynolds number based on wagon width of $Re_w = 0.3 \times 10^6$, matching the wind-tunnel experiment.

For case 2, a domain with similar cross section to that used for case 1 was used, but with a reduced length of $C = 38.84W$, to reduce computational cost. The inlet condition of case 2 was based on the experimental boundary-layer profile measured using a cobra probe at the middle of the top surface of the second wagon for the gap combination $G_f = 0.3W$ and $G_b = 0.3W$. The ground clearance and 1% turbulence intensity of the numerical domain were chosen to match the wind-tunnel tests. A no-slip boundary condition was used at the bottom of the domain. Symmetry conditions were employed for all the steady-RANS simulations. A zero-shear wall condition for the top and side walls was applied.

Embedded Large Eddy Simulation (ELES) is a zonal LES method, which employs a larger RANS computational domain in order to better match turbulence inflow statistics at a computational inlet of the LES domain. It does this by using the RANS model to construct time-dependent turbulence, either through adding in the effect through a collection of point vortices or using a synthetic turbulence generator (Mathey et al., 2003). This provides a truer representation of the time-dependent inflow turbulence of real physical systems. In order to conduct the ELES simulation, the RANS and LES zones were predefined through splitting the domain into RANS and LES regions, as depicted in Fig. 1. The RANS/LES interfaces of cases 1 and 2 were located at $4W$ and $10.23W$, respectively, upstream of the test wagon. The lengths of the LES domains in the spanwise direction for cases 1 and 2 were $4W$ and $4.5W$. It should also be noted that another aim of using the ELES approach is to reduce the cost of LES, over using it for the entire domain. Hence, the size of the embedded LES domain should be selected cautiously to avoid the high computational cost of pure LES, while still accurately capturing the highly time-varying flow around the model. The influence of the size of LES domain is explicitly discussed in Section 5.1.4.

4. Numerical method

Similar to the wind tunnel test, all 49 different gap size combinations were simulated, in this case using the RANS *SST* (Shear Stress Transport) $k-\omega$, Realizable $k-\varepsilon$ and RSM ((Full) Reynolds Stress Model), due to their relatively cheap computational cost. The results computed by the *SST* $k-\omega$ and Realizable $k-\varepsilon$ are not reported here due to similarity to those from RSM. Hence, the RANS results presented in this study refer to the RSM model. For the computations, the commercial flow simulation package ANSYS FLUENT version 16.1 was used. The equations were solved using the coupled algorithm. The enhanced wall treatment (EWT) was used for regions adjacent to solid surfaces to ensure that the appropriate turbulence equilibrium conditions were applied at the first grid point adjacent to the wall.

For the transient simulations of the cases 1 and 2, three widely used unsteady turbulence models, ELES, SAS and URANS were employed. The SIMPLEC algorithm was utilised for time integration. The transient simulations undertaken for cases 1 and 2 are listed in Table 1. The *SST* $k-\omega$ model was chosen as the RANS model for the SAS and URANS cases. Due to high cost of resolving the near-wall region at the Reynolds number studied, the WMLES model was selected to reduce the mesh resolution requirement of LES at the wall. WMLES models the flow close to the wall based on a RANS mixing length model, and resolves the central part of the boundary layer with LES allowing for a coarser near wall grid resolution than in the LES requirements. The vortex method was applied at the RANS/LES interface to introduce synthetic turbulence. The added perturbations were generated through a number of discrete vortices providing turbulent fluctuations at the inlet of the LES zone. This

[1] This device could measure three velocity components in a flow with an acceptance cone angle of 45° and velocity up to 50 m/s, and has a frequency response up to 2000 Hz.

Table 1
List of transient simulation cases. Top: single wagon; Bottom: multiple wagons with gap combination $G_f = 9.38W$ and $G_b = 3.23W$.

Single Wagon	Elements	0.015 T_{ref}	0.006 T_{ref}
Fine	13 million		ELES-4W-1.55H[a]
	9.5 million	SAS	SAS
Medium	6.5 million	SAS	SAS
	5 million	ELES-4W-1.55H[a]	
Coarse	4.5 million		SAS
$G_f = 9.38W$ and $G_b = 3.23W$	Element	0.015 T_{ref}	0.006 T_{ref}
Fine	18.5 million		ELES-4.5W-1.5H[a]
	18 million		ELES-4W-1.65H[a]
	17 million		ELES-4W-1.5H[a]
	16 million		ELES-2.5W-1.5H
	11 million	URANS & SAS	URANS & SAS
Medium	6.5 million	URANS & SAS	URANS & SAS
Coarse	4.5 million	URANS & SAS	URANS & SAS

[a] Non-conformal mesh.

injection allows the balance between RANS and LES turbulent content across the interface to be preserved.

The time-averaged pressure distribution calculated in this study is expressed in terms of local pressure coefficient. This is defined as

$$C_p = \frac{P_t - P_{\text{ref}}}{0.5\rho U_\infty^2}. \quad (1)$$

Here, P_t is the time-averaged static pressure, U_∞ is the uniform wind speed, ρ is the density and P_{ref} is a suitable reference pressure.

In order to calculate the pressure drag coefficient (C_{DP}), the pressure is integrated over the front and base surface to give an area-averaged pressure coefficient (C_P). The difference between the front surface pressure coefficient (C_{Pfront}) and base surface pressure coefficient (C_{Pbase}) gives the pressure drag coefficient of the wagon C_{Dp},

$$C_{Dp} = C_{Pfront} - C_{Pbase}. \quad (2)$$

4.1. Grid resolution

ANSYS ICEM-CFD software was employed to construct meshes with different grid resolutions for cases 1 and 2. Two grids with approximately 3 and 4.5 million cells were constructed for the steady-RANS simulations. Only a 0.2% difference in pressure drag coefficient was observed in increasing the number of cells from 3 to 4.5 million. Hence, the grid with 3 million cells was chosen as sufficient for the case with gap combination $G_f = 9.38W$ and $G_b = 3.23W$ for the RANS computations. It should be noted that a higher number of cells was used for the larger inter-wagon gaps, e.g., for $G_f = 12.61W$ and $G_b = 12.61W$, 3.6 million cells were used.

For the single wagon case, the meshes for the SAS runs had 4.5, 6.5 and 9.5 million cells, corresponding to the *coarse*, *medium* and *fine* grid cases, respectively. Meshes for the single wagon ELES cases had approximately 5 and 13 million cells. The size of LES domain in the spanwise and vertical direction was 4W and 1.55H, respectively. For case 1 only, temporal and spatial resolution for the ELES approach will be discussed in Section 5.1.2. However, it should be noted, similar to case 2, considerable care was taken to generate a near-optimal mesh for case 1.

Table 2 lists the essential input and output information for computations with the different grid resolutions and different turbulence

Table 2
Drag predictions for case 2 as a function of turbulence model, and mesh and time resolution.

$G_f = 9.38W$ and $G_b = 3.23W$	Mesh	Elements	T_{ref}	C_{Dp}	% Experiment
Experiment	–	–	–	0.731	–
ELES-4.5W-1.5H[a]	Fine[b]	18.5 million	0.006	0.744	1.7%
ELES-4W-1.65H	Fine[b]	18 million	0.006	0.750	3%
ELES-4W-1.5H	Fine[b]	17 million	0.006	0.760	3.8%
ELES-2.5W-1.5H	Fine	16 million	0.006	0.770	5.2%
SAS-CD[a]	Fine	11 million	0.006	0.761	4%
SAS-BCD[a]	Fine	11 million	0.006	0.717	2%
SAS-BCD	Fine	11 million	0.015	0.771	5.2%
SAS-BCD	Medium	6.5 million	0.006	0.761	4%
SAS-BCD	Coarse	4.5 million	0.006	0.759	3.7%
URANS[a]	Fine	11 million	0.006	0.724	−0.9%
URANS	Fine	11 million	0.015	0.733	0.4%
URANS	Medium	6.5 million	0.006	0.711	−2.8%
URANS	Coarse	4.5 million	0.006	0.700	−4.4%
RANS[a]	Fine	3 million	–	0.520	−40.6%

[a] Representative cases.
[b] Non-conformal mesh.

models. In particular, it provides a comparison of the pressure drag coefficient predictions against the experimental value for case 2. For the multiple wagon setup with $G_f = 9.38W$ and $G_b = 3.23W$, the total number of cells generated for URANS and SAS were approximately 4.5, 6.5 and 11 million, for the coarse, medium and fine grids, respectively. Due to the complexity of upstream flow condition for this multiple wagon setup, four different grids were constructed to find the optimal size for the embedded LES domain, by varying the spanwise and vertical extent. Embedded LES domains with widths and heights of $2.5W$ & $1.5H$, $4W$ & $1.5H$, $4W$ & $1.65H$, and $4.5W$ & $1.5H$ were generated, with approximately 16, 17, 18 and 18.5 million cells, respectively. An example of the meshing strategy used to capture the critical flow regions for the full train model is shown in Fig. 2.

Furthermore, different locations for the RANS/LES interface were tested to find the most economical size for the LES domain in the streamwise direction. Recall that the RANS/LES interface is used to introduce synthetic turbulence in the LES flow domain, which could be expected to alter the flow development after the upstream boundary layer separates as the fluid advects into the upstream gap (G_f). Not surprisingly, it was found when the RANS/LES interface was located inside the front gap, the introduced synthetic turbulence (matching the RANS model) took some time to readjust leading to under predicting the pressure drag coefficient, C_{Dp}, and the front surface pressure. Thus, a good compromise position for the RANS/LES interface was found to be slightly upstream of the front gap.

The structured hexahedral method was employed for generating the SAS, URANS and RANS grids, while the non-conformal method with hexahedral cells was used for generating the ELES grids. The latter method saved at least 25% of total number of elements compared to the former, allowing in increase the size of LES domain in the spanwise direction from $2.5W$ to $4W$ without an increase in the total number of cells generated. The constructed finest meshes showed y^+ varied between 1 and 14 over the surfaces of the wagons.

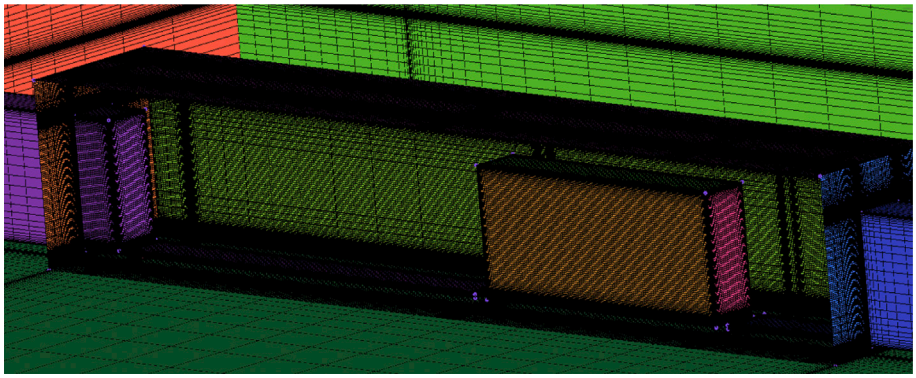

Fig. 2. Fragment of ELES non-conformal fine mesh of multiple wagon setup (case 2) with gap ratio combination $G_f = 9.38W$ and $G_b = 3.23W$. The LES zone is shown.

4.2. Timestep resolution

The URANS and SAS simulations were performed using two timesteps, as shown in Table 1. The timestep was normalised by T_{ref}, which is equivalent to the time taken for the fluid to advect one wagon length at the freestream velocity. Time-averaged results are obtained through averaging the flow over $50T_{\text{ref}}$, after the flow was checked to be dynamically steady through comparing averages based on smaller averaging times.

The timesteps selected for URANS and SAS simulations are equivalent to 0.015 T_{ref} and 0.006 T_{ref}. These timesteps give maximum Courant numbers of $\sim$ 12 and 6, respectively, although they are only greater than one over very limited locations in the near wall regions. As URANS cannot resolve small-scale features (Sagaut et al., 2013), no further timestep or grid refinement was pursued for that case.

For the SAS approach, the timestep has an explicit impact on the formation of the resolved turbulent structures in unstable flows (Menter and Egorov, 2010). The SAS model is probably the most robust global (or non-zonal) RANS/LES approach relying on a single set of equations that blends into a generalized model RANS and LES model (Sagaut et al., 2013). The SAS approach is based on the K-KL model of Rotta, where K and L are the turbulent kinetic energy and turbulent length-scale, respectively. The idea behind SAS is the introduction of the von Karman length-scale by retaining the second derivative of the K-KL equation (Frohlich and von Terzi, 2008). Hence, SAS contains two length-scales, the one related to the first derivative of the resolved velocity, and a second one related to the higher derivatives of the resolved velocity (Frohlich and von Terzi, 2008). Through the mathematical blending function, SAS can calculate a different length-scale according to which of the models provides the larger length-scale. This functionality allows SAS to acts in RANS mode near the wall and switch to LES where unsteadiness is detected. A limitation however, is that utilising SAS where the underlying flow instability is not very strong, can prevent the switch to LES causing SAS to remain in URANS mode, possibly giving even poorer results than URANS (Davidson, 2006). The flows here have fixed separation points and thus lead to strongly unstable wakes. Thus SAS does switch to LES mode automatically in the wake. In addition, Central Differences (CD) were used for the advective terms in the Navier-Stokes equations, rather than the slightly more dissipative scheme, Bounded Central Differences (BCD) for which switching was problematic. This leads to a better prediction against experiments.

5. Results and discussion

The capability of different turbulence models for predicting the flow and aerodynamics forces for the single wagon (case 1), and multiple wagons configured with gap combination $G_f = 9.38W$ and $G_b = 3.23W$ (case 2), is discussed here. In section 5.1, C_p on the centreline of the front, top and base surfaces of the wagon for cases 1 and 2 are compared based on grid resolution and timestep selection, and the size of LES domain. In sections 5.2 and 5.3, the pressure drag coefficient and the time-averaged pressure coefficient, surface-pressure contours, and side and top skin-friction lines for cases 1 and 2 are compared with the wind tunnel results. The numerical time-averaged streamwise velocity profile above the top of the wagon and in its wake are also presented in the section 5.3. In section 5.4, the pressure drag coefficient, C_{Dp}, computed using RANS simulations for multiple wagons with various gap sizes is examined. Finally, in section 5.5, the computational cost of all models studied in this paper are provided and discussed, with a view to analysing the cost/benefit, which depends on which predicted variables are required.

5.1. Resolution and domain studies

In this section, the pressure drag coefficient, C_{Dp}, and pressure coefficient, C_p, on the centreline of the front, top and base surfaces of the wagon for both cases are compared based on grid size and timestep, and the size of LES domain.

5.1.1. Grid resolution and timestep selection for case 1 (single wagon)

Fig. 3 shows the effect of the ELES temporal and spatial resolution on the pressure coefficient, C_p, on the centreline of the front, top and base surfaces for the single wagon case. Despite a two and half times increase in the number of grid points and a decreased timestep, very little change can be observed over the perimeter of the wagon. A slight difference between the two cases is the better match with experiments for the recirculating flow and the position of the reattachment point at the top of the wagon. Note that for this comparison, the reference static pressure was taken at the centreline point 0.75 wagon lengths downstream of the leading edge. This was far enough downstream to allow the boundary layer to recover from the upstream separation/recirculation. This same point was used for both the experimental and numerical C_p. This reflects that fact that wind tunnels generally have a non-negligible pressure gradient in their working section, while numerical flow predictions usually don't, thus this choice for P_{ref} tends to minimise the effect of the wind tunnel pressure gradient adversely affecting the comparison, which would result if a standard upstream wind-tunnel static-pressure reading was used as a reference value.

5.1.2. Influence of grid resolution for case 2 (multiple wagons)

The contribution of grid resolution on the pressure drag coefficient, C_{Dp}, for URANS and SAS-BCD simulations are shown in Table 2. Less than a 2% change in the pressure drag coefficient is observed between the URANS medium and fine mesh predictions, while the difference between SAS-BCD medium and fine grids predictions is approximately 5%.

The influence of grid refinement on the pressure coefficient, C_p, on the centreline of the front, top and base surface of the wagon, is presented in Fig. 4. As expected, the SAS-BCD model shows a higher dependency on grid size compared to URANS, particularly on the front surface of the

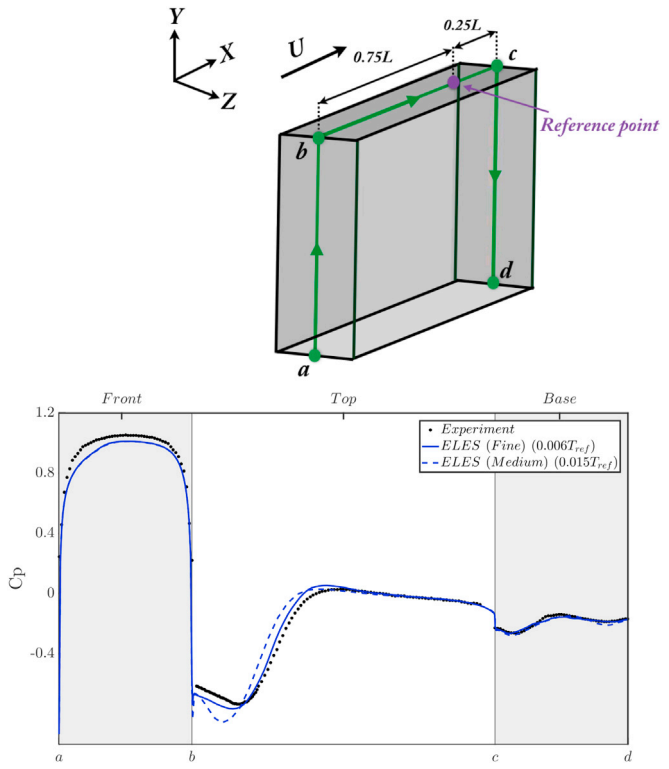

Fig. 3. Coordinate system and the reference point used in the present study (top), Time-averaged surface pressure coefficient, C_p, of the single wagon case (case 1) along the centreline ($z = 0$) (bottom).

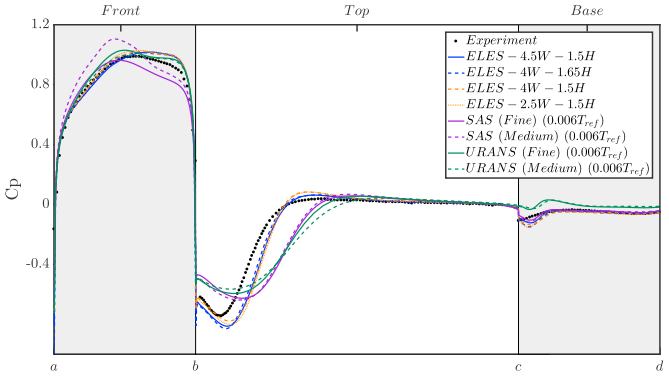

Fig. 4. Time-averaged surface pressure coefficient, C_p, variation along the centreline of the test wagon for different grid resolutions for case 2.

wagon. It is thought that having a coarser grid upstream of the test wagon, inside the upstream gap, delays the switch from RANS to LES mode to occur.

5.1.3. Influence of timestep for case 2 (multiple wagons)

The effect of the timestep on the pressure drag coefficient, C_{Dp}, and pressure coefficient, C_p, on the centreline of the front, top and base surface of the wagon for case 2 for the URANS and SAS-BCD simulations are presented in Table 2 and Fig. 5. It is apparent that the accuracy of the URANS results is only weakly dependent on the timestep, as expected. However, the contribution of a timestep change to the computed pressure drag coefficient for the SAS-BCD model is almost 7%. This high SAS dependency on timestep is more evident on the front surface of the wagon, indicative that the state of the flow inside the front gap is not accurately captured unless the timestep is small enough.

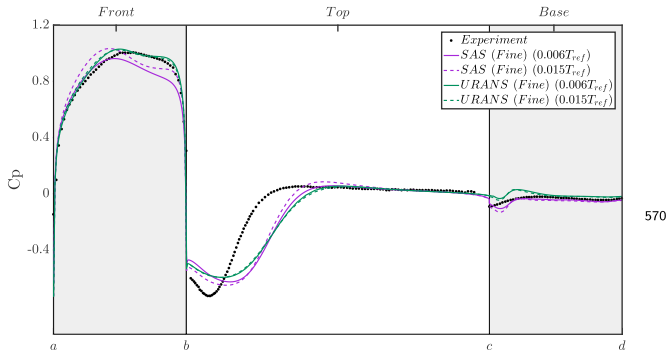

Fig. 5. Time-averaged surface pressure coefficient, C_p, variation along the centreline of the test wagon. This figure shows the effect of different timesteps on the predictions for case 2.

5.1.4. Influence of the size of LES domain

The influence of the embedded LES domain dimensions in the spanwise and vertical directions on the C_{Dp} and C_p can be observed in Table 2 and Fig. 4. The effect of an increase in the LES domain span from 4W to 4.5W and height from 1.5H to 1.65H is less than 2% for the pressure drag coefficient. Fig. 4 shows a very little difference between the C_p on the centreline of the front, top and base surfaces obtained from all ELES cases using different sized LES domains. The similarities of the ELES results suggest that any further increase of the LES domain size would have negligible effect on the ELES predictions. This is an indication that the main unsteady (turbulent) flow structures are well contained in the range of LES domains chosen for this study. The effect of an increase in the LES domain size in the streamwise direction was discussed earlier in Section 4.1.

5.2. Single wagon in free-stream

Further details of the numerical predictions using different turbulence models for an isolated double-stacked wagon in free-stream are discussed in this section. The models considered were ELES, SAS-BCD, SAS-CD and RANS. URANS was also used for case 1 but it was found that the predicted wake remained steady and symmetric.

5.2.1. Embedded LES

As expected, all numerical models predict similar front pressure distributions to the wind tunnel data (not shown here). Figs. 6 and 7 present a wind-tunnel surface-flow visualisation (skin-friction lines) and the numerical time-averaged side and top streamlines for the different models. The wind-tunnel surface-flow visualisation was obtained using Kaolin china clay 340 mixed with kerosene and fluorescent dye. The final experimental images obtained were enhanced with UV light. It can be seen ELES accurately predicts the separating shear layers rolling up into two small and large recirculation bubbles on the side and top surface of the wagon. The recirculating structures computed with ELES are in good agreement with the wind-tunnel reattachment lines, R1 and R2, for both the side and top surfaces. The maximum reattachment length of R2 reported by Li et al. (2017) was approximately 0.4L, which is very similar to the ELES prediction.

The effect of the top and side flow features are illustrated in Fig. 8. The pressure coefficient, C_p, computed by ELES displays very similar pressure recovery indicative of reattachment compared to the wind-tunnel results on both surfaces. It is speculated, the reason why the ELES side C_p matches slightly better with the wind tunnel results than the ELES top C_p is due to the larger distance of the side surface of the wagon to the wind tunnel side walls compared to the top surface of wagon to the roof of the wind tunnel. In other words, the boundary layers on the side surfaces of the wagon was less influenced by the wind tunnel side walls than the boundary layers on the top surface of the wagon.

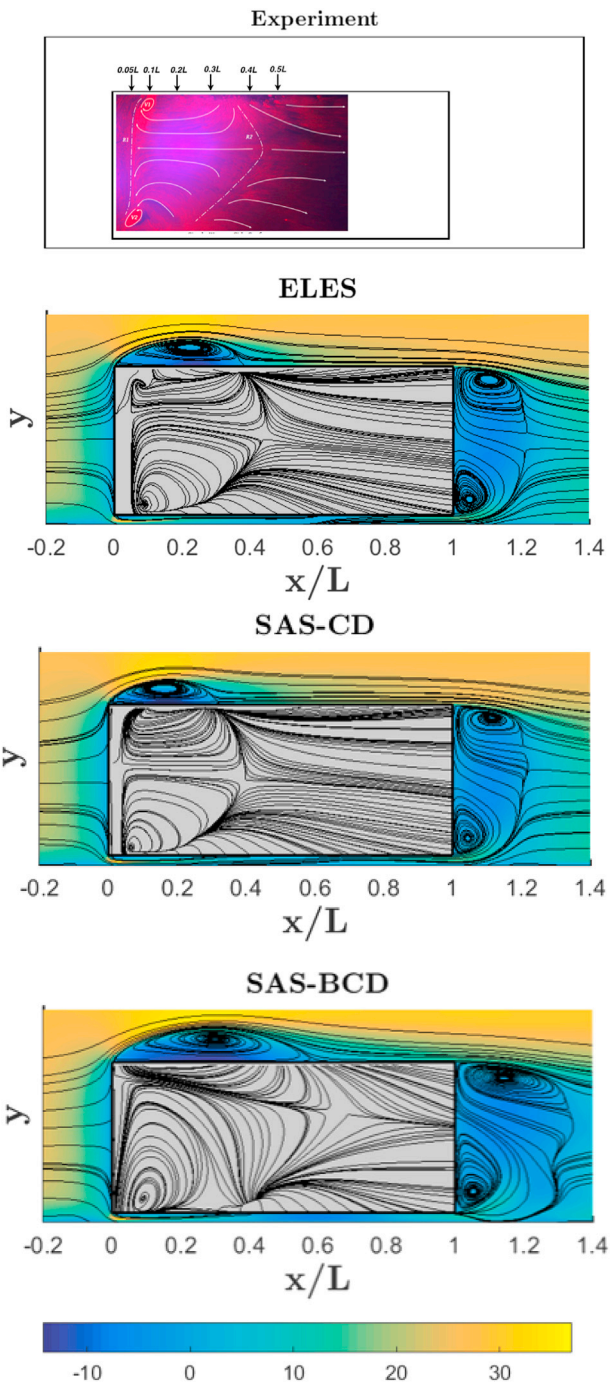

Fig. 6. Time-averaged streamlines for the single wagon (case 1) on x-y plane at $z = 0$ (side surface).

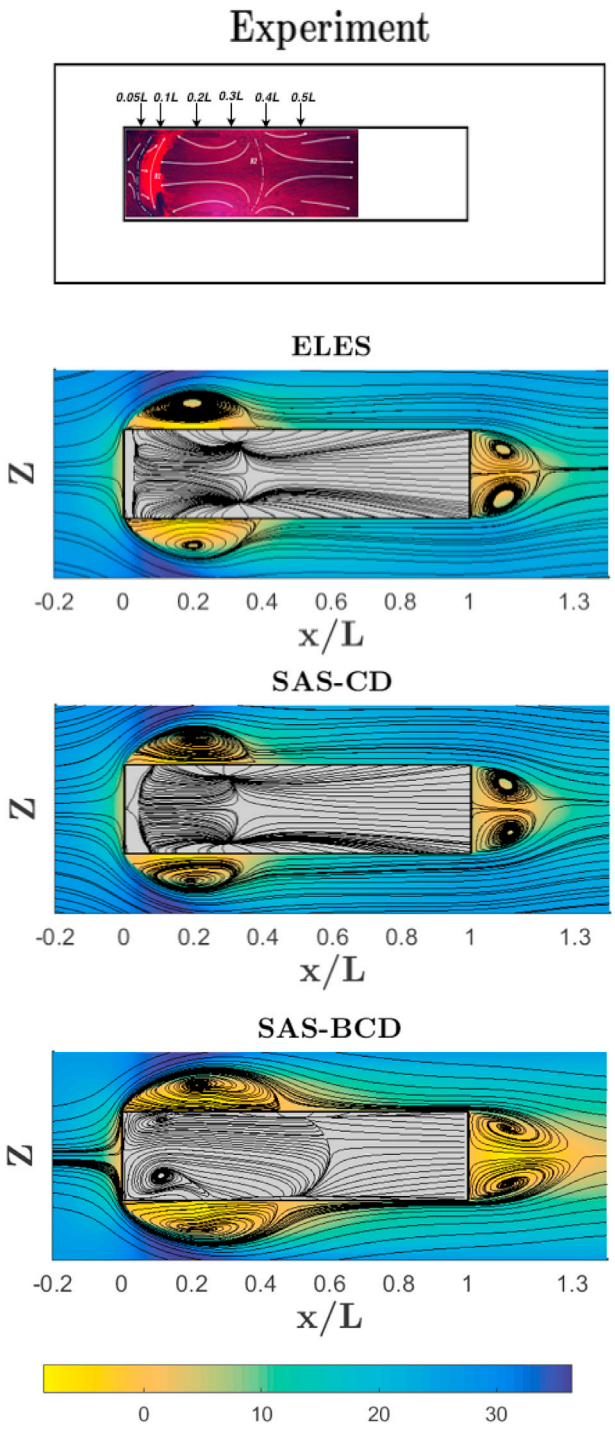

Fig. 7. Time-averaged streamlines for the single wagon (case 1) on x-z plane at $y = H/2$ (top surface).

Fig. 9 illustrates that ELES captures the correct pressure distribution on the base surface of the single wagon case. Consequently, the pressure drag coefficient predicted by ELES is within 1% of the experimental value, as presented in Table 3. The ELES results for case 1 confirm that size of LES domain was appropriate to provide sufficient space for the turbulent flow to be fully developed upstream of the wagon.

5.2.2. RANS

While RANS correctly predicts the front pressure distribution, it performs unsatisfactorily for providing the reattachment point on the top and side surfaces. In particular, it over-predicts the length of recirculation bubble. Additionally, RANS under predicts the pressure on the base surface resulting in 12.5% difference in the pressure drag coefficient compared to the experimental value, as shown in Table 3. The inability of RANS to predict a flow field with substantial separation is well-known and in agreement with other studies. Ashton et al. (2016) assessed the capability of RANS and DES against experimental data for the Ahmed body and a more realistic automotive vehicle model – the DrivAer model[2]. They used meshes with 16 and 80 million cells for the Ahmed body, and the fastback and estate DriveAer configurations, respectively.

[2] DriveAer (Lienhart and Becker, 2003) is an open source car model based closely on realistic complete car geometries with openly available experimental data.

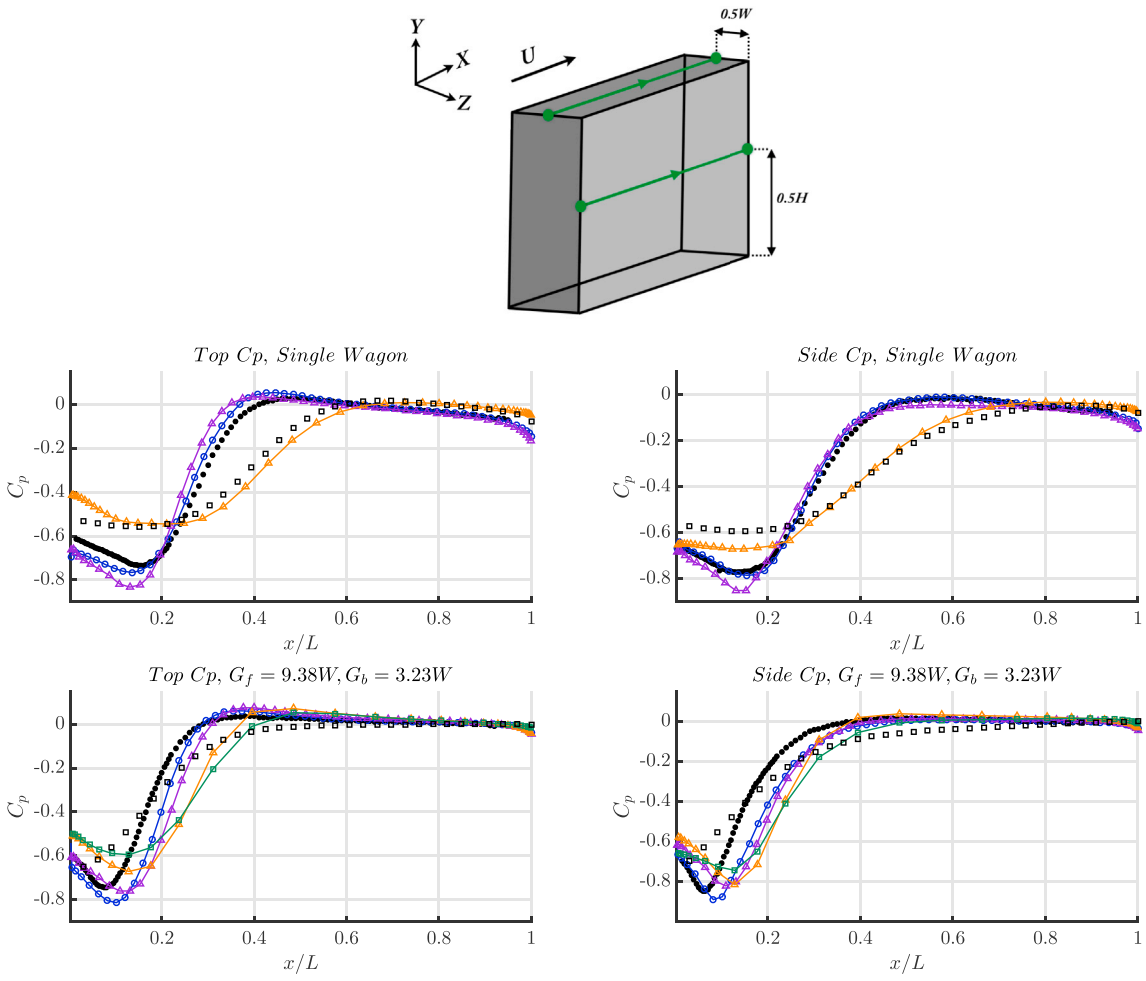

Fig. 8. Top C_p for single wagon (top left), Side C_p for single wagon (top right), Top C_p for gap combination $G_f = 9.38W$ and $G_b = 3.23W$ (bottom left) and Side C_p for gap combination $G_f = 9.38W$ and $G_b = 3.23W$ (bottom right).

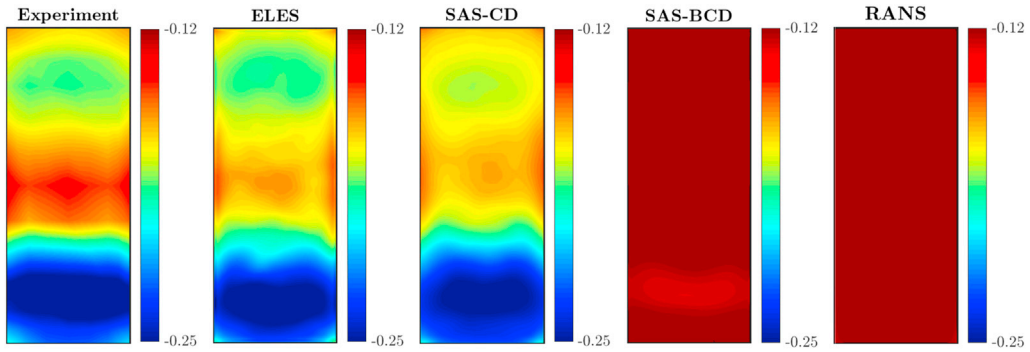

Fig. 9. Time-averaged single-wagon base surface pressure.

Table 3
Pressure coefficients on the front and back faces for the single wagon.

Single Wagon	Experiment	ELES	SAS-CD	SAS-BCD	RANS
C_{Dp}	0.93	0.923 0.8%	0.938 0.9%	0.775 20.7%	0.833 12.5%

They reported the inability of RANS to capture the flow field for both models, regardless of mesh resolution.

5.2.3. SAS

The current set of simulations indicate that most flow measures computed using SAS with the BCD scheme, such as the pressure drag coefficient, base pressure contours and the size of recirculation bubble on top and sides of the wagon, are similar to the RANS predictions. This similarity is due to a known problem encountered with the SAS approach. In situations that are not strongly globally unstable, SAS may stay in RANS mode rather than switching to scale-resolving LES mode. Given that the wake flow is strongly time-dependent in reality, this would seem

to suggest that the problem could be the extra dissipation induced by the BCD scheme. Davidson (2006) investigated the flow in an asymmetric diffusor to compare the results of SAS to URANS. He found the model did not run either in URANS nor LES modes, but somewhere in between. This resulted in poorer results than URANS.

However, the flow field calculated by SAS with the CD scheme agrees well with both the wind tunnel and ELES results. It predicts a similar pressure drag coefficient, C_{Dp}, and base pressure contour to the ELES and wind tunnel results. Similar to the wind tunnel flow visualisation, the two small and one large recirculation bubbles on the side and top surface of the wagon can be seen on the surface streamline plots computed by SAS-CD. As shown in Fig. 8, the flow reattachment point computed by SAS-CD on the top and side surfaces are closely matched with the wind tunnel and ELES results. These results suggest the use of a less dissipative scheme triggers unsteadiness around the wagon, and thereby the switch from RANS to LES mode could occur leading to resolving the large turbulent scales and indeed part of the turbulence spectrum. The ability of the SAS model to provide very similar predictions to ELES makes it a very attractive approach. It should be noted that SAS not only does require less care to be taken for setting up a case than ELES, but also the cost of SAS is significantly lower than ELES.

5.3. Multiple wagons at $G_f = 9.38W$ and $G_b = 3.23W$

As mentioned above, only a single multiple wagon case was computed ($G_f = 9.38W$ and $G_b = 3.23W$) using the three turbulence models: ELES, SAS, and URANS, due to high computational cost of transient simulations. Fig. 10 illustrates the comparison between the numerical and experimental front and base pressure contours. While the front surface pressure is correctly computed by all transient models, the steady RANS model fails to even predict the stagnation point on the surface.

Figs. 11 and 12 illustrate a good qualitative agreement of ELES and SAS-CD with the wind-tunnel surface visualisation. They both show a similar position for the reattachment line, R2, and correctly predict the maximum length of recirculation bubble is almost 0.28L on the top and side surfaces. However, URANS and SAS-BCD over-predict the recirculation structure on both surfaces.

Fig. 8 provides another comparison of the accuracy of the numerical models in predicting the behaviour on top and side of the wagon. It is apparent ELES provides the most accurate prediction amongst all models by computing a similar length of the recirculation bubble and reattachment point on both surfaces. The SAS-CD model predicts a very similar reattachment point on the top surface to the wind tunnel and ELES results. The SAS-BCD and URANS models perform unsatisfactorily by over-predicting the size of mean recirculation bubble on top and side surfaces of the wagon. RANS provides the least accurate prediction by computing the largest recirculation bubble on both surfaces.

The wind-tunnel boundary-layer profiles measured above the top surface and in the wake of the wagon were compared across all the numerical models. Fig. 13 displays the XY planes used for the streamwise velocity comparison. Nine locations at the top surface of the wagon, $x = 0L$, $0.3L$, $0.4L$, $0.5L$, $0.6L$, $0.7L$, $0.8L$, $0.9L$ and $1L$, are compared, as shown in Fig. 14. The majority of data at $x = 0.2L$, passing through the recirculation region, have less than 80% quality, and therefore are not shown. This is caused by the failure of the Cobra probe to measure velocities outside its 45° acceptance cone. All numerical approaches show a similar boundary layer profile at $x = 0L$, equivalent to the leading edge of the wagon where separation occurs. Although ELES and SAS-CD display the shear-layer reattachment at $x = 0.3L$, corresponds to the downstream edge of recirculation bubble in the experiment, they under-predict the streamwise velocity slightly at this location. SAS-BCD, URANS and RANS over-predict the length of recirculation bubble, showing the reattachment occurs approximately at $x = 0.4L$. While slightly under-predicted, the velocity profiles computed by ELES and SAS-CD from $x = 0.5L$ to $x = 1L$ are in a good agreement with the wind tunnel data. SAS-CD predicts almost identical streamwise velocity profiles compared to ELES over this range indicating the switch from RANS to LES mode has correctly occurred. This in turn leads to a very good pressure recovery prediction, and subsequently computation of an accurate surface pressure distribution and pressure drag coefficient.

Comparisons between numerical and wind-tunnel streamwise velocity profiles in the wake of the wagon at 6 locations: $x = 1.05L$, $1.1L$, $1.2L$, $1.3L$, $1.4L$ and 1.5L are presented in Fig. 15. While all numerical predictions show some differences at $x = 1.05L$, $1.1L$ and $1.2L$, which is close to the trailing edge of the wagon where separation occurs, ELES and SAS-CD predictions are much closer, both in this region and further downstream, than URANS and RANS.

The numerical base C_P contours are shown in Fig. 10. Similar to the single-wagon case, the base C_P distribution and the pressure-drag coefficient computed by ELES are in the closest agreement to the wind tunnel

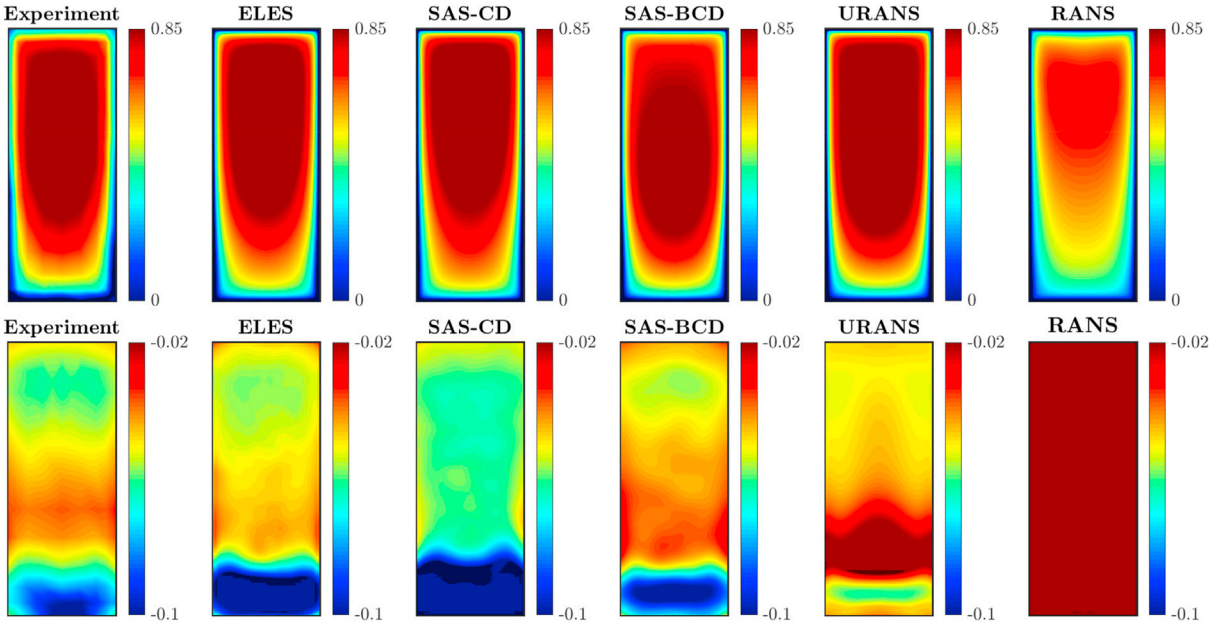

Fig. 10. Pressure coefficient (C_p) distribution on the front (top) and back (bottom) surfaces, presented for gap combination $G_f = 9.38W$ and $G_b = 3.23W$.

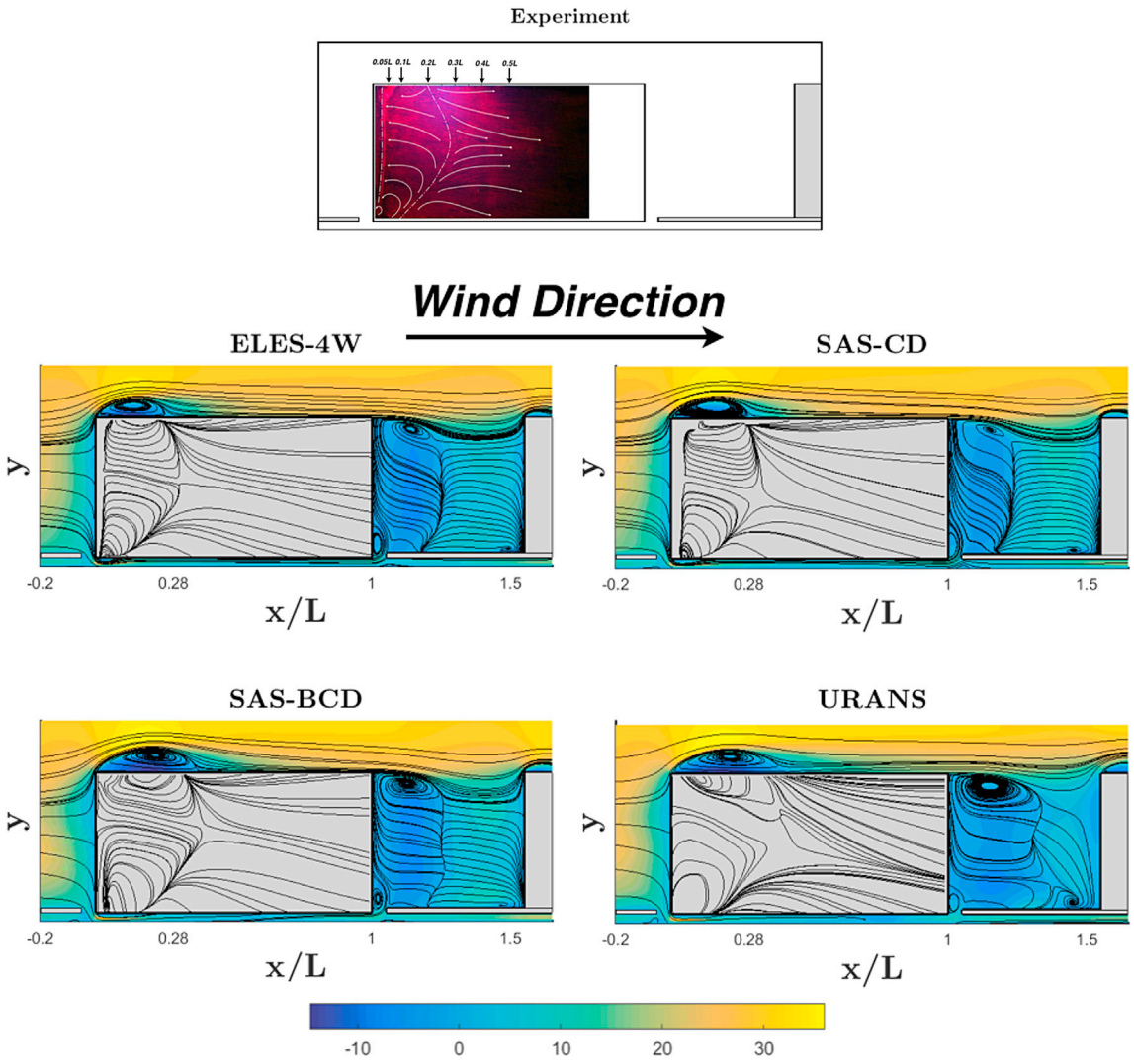

Fig. 11. Wind-tunnel surface visualisation on the side surfaces (top); predicted time-averaged surface streamlines (bottom). Gap combination $G_f = 9.38W$ and $G_b = 3.23W$ (case 2) on x-y plane at $z = 0$.

result among other numerical model predictions. The ELES prediction of the pressure distribution across the base surface matches well with the experimental measurements in both overall magnitude and distribution. This would seem to be an indication that the flow structure within the rear gap is well predicted. However, experimental velocity fields within the gap were not available to test this hypothesis. Table 2 shows the pressure drag coefficient difference between ELES and the experiment is less than 2%. In contrast to the single wagon case, both SAS-CD and SAS-BCD present the similar base pressure distribution compared to the wind tunnel, while SAS-BCD displays a slightly closer qualitative agreement, which clarifies its 2% better C_{Dp} prediction compared to SAS-CD, shown in Table 2. This relatively accurate prediction by SAS-BCD happens due to the high turbulent region upstream the wagon, inside $G_f = 9.38W$, which causes the switch from RANS to LES mode to occur further upstream of the wagon. Hence, the large turbulent scales responsible for carrying eddies inside $G_f = 9.38W$ are resolved before flow impinges on the front surface of the wagon. However, it is concerning that the SAS-BCD prediction is better than the SAS-CD prediction, given that a reasonably fine grid is used.

As expected, RANS performs unsatisfactorily for predicting the base C_P contours, and subsequently C_{Dp}. RANS under-predicts the pressure drag coefficient by almost 40%. The reasons why RANS fails to even predict the medium-scale turbulent features are discussed above in Section 5.2.2.

Apart from the close C_{Dp} prediction, other parameters calculated using URANS show discrepancies with the experimental data. Hence, it is assumed that URANS's good C_{Dp} prediction is possibly fortuitous, and it may not provide a reasonable pressure drag prediction for other gap size combinations. To investigate this further, the gap ratio combination $G_f = 1.77W$ and $G_b = 3.23W$ was modelled with URANS using approximately 11 million cells. Almost an 8% C_{Dp} difference was found, considerably worse than the case 2 prediction.

5.4. RANS simulations of all gap sizes

All 49 upstream and downstream gap spacing combinations tested experimentally were simulated using (steady) RANS, as described in Section 4. Fig. 16 presents the changes in pressure drag coefficient for the various gap combinations computed by RANS and measured experimentally. Although RANS under-predicts the pressure drag coefficient for the various gap combinations compared to experiments, it computes a similar drag contour map variation. Additionally, RANS predicts a higher drag penalty occurs due to increasing the gap size in agreement with the wind tunnel tests. Furthermore, the RANS results show the effect of an increase in G_f on the drag penalty is much higher than the impact of an increase in G_b.

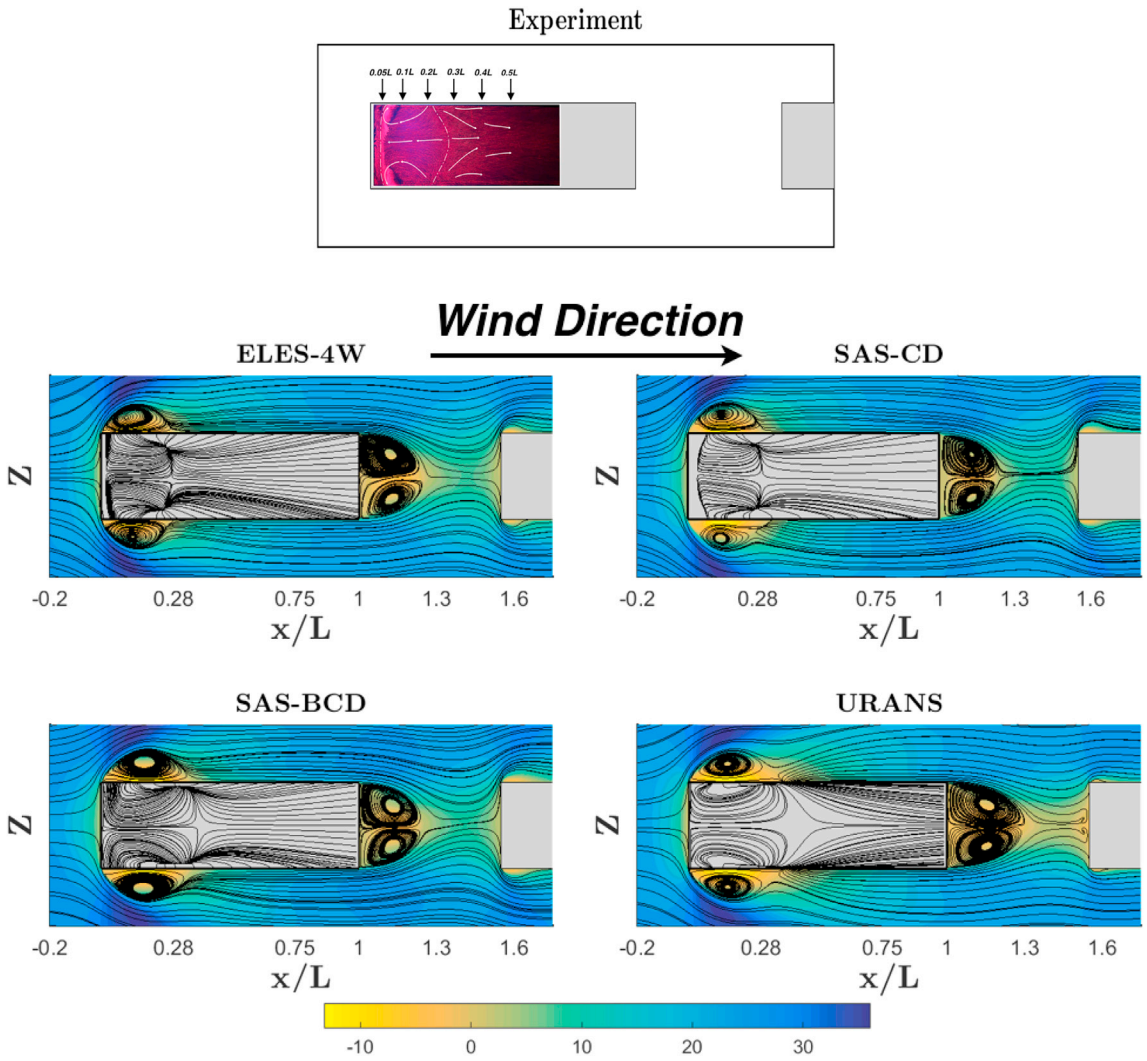

Fig. 12. Wind-tunnel surface visualisation on the top surface (top); time-averaged surface streamlines (bottom). Gap combination $G_f = 9.38W$ and $G_b = 3.23W$ (case 2) on x-z plane at $y = H/2$.

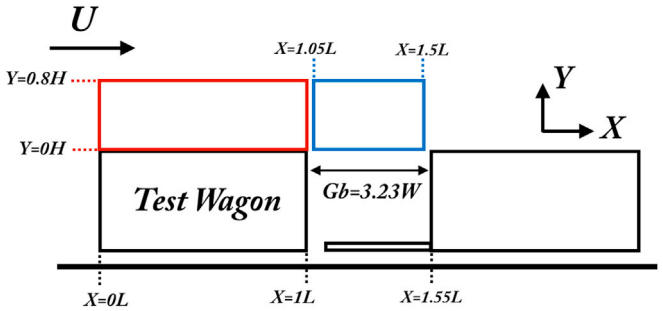

Fig. 13. The red XY planar section at $Z = 0$ was used to record streamwise velocity profiles at the top of the test wagon. The blue XY planar section at $Z = 0$ was used for wake measurements. (For interpretation of the references to colour in this figure legend, the reader is referred to the web version of this article.)

5.5. Computational expense

Although the ELES and SAS methods have proved to the provide more accurate results relative to URANS and RANS, the computational cost of each model should also be considered for engineering applications. Table 4 presents the CPU time used for all turbulence models employed for case 2. The cost of RANS is approximately 1/33th and 1/66th of SAS-CD and ELES-4.5W-1.5H, respectively. Indeed, the overall relative cost of RANS may be even better, given that a coarser mesh may work just as well. This suggests RANS is the most attractive approach among other numerical models for this engineering application if drag is the main parameter of importance, due to its cheap computational cost and its relatively accurate prediction of the relative drag of different gap combinations. It is expected RANS would be able to predict the pressure drag coefficient with an acceptable precision for the multiple wagons at various gap sizes provided that an accurate fully developed turbulent profile was simulated upstream of the front gap. In future work, it is planned to use Particle Image Velocimetry (PIV) to obtain the turbulent velocity profile slightly upstream of the largest front gap. It is conjectured that better turbulent profile at the inlet of computational domain would improve the accuracy of the RANS drag prediction.

On the other hand, it may be valuable to better understand the flow in the gaps and its effect on the surface pressure distributions, as it may provide opportunities to explore passive or active control methods to reduce overall drag. In such a case, it is clearly useful to know that the ELES and SAS predictions provide a truer representation of the surface pressure, and by implication, the separated flows. In addition, the ELES and SAS models predict the pressure drag much more accurately, so if absolute values are required rather than relative trends, then these more expensive methods may be needed.

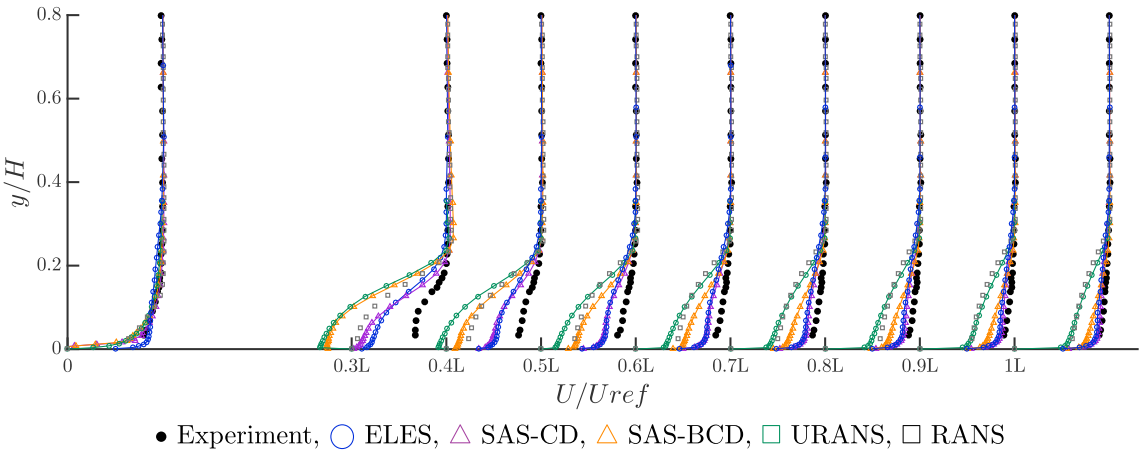

Fig. 14. Time-averaged streamwise velocity at the top of wagon at $G_f = 9.38W$ and $G_b = 3.23W$.

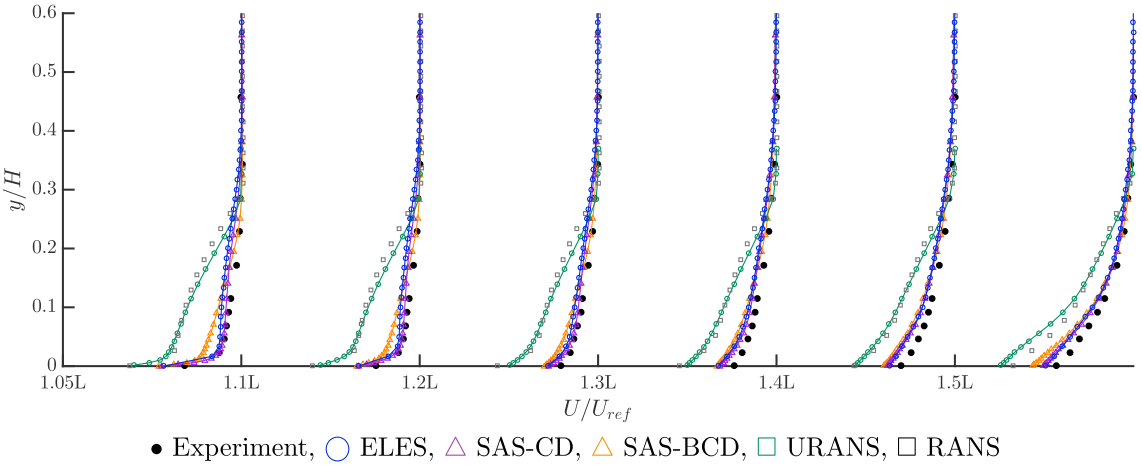

Fig. 15. Time-averaged streamwise velocity in the wake at $G_f = 9.38W$ and $G_b = 3.23W$.

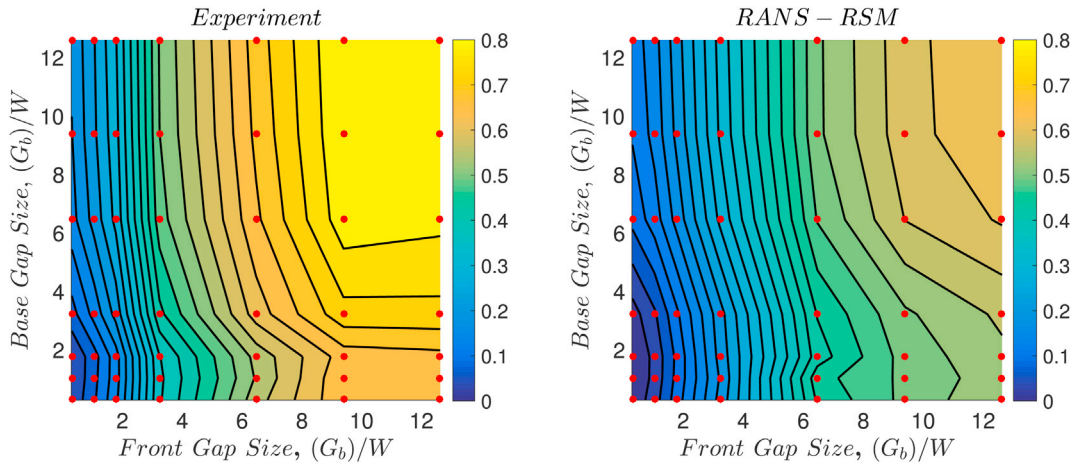

Fig. 16. Contour plot of pressure drag coefficient C_{DP} with respect to varying combinations of front (Gf) and base (Gb) gap sizes. Experiment (left), RANS-RSM (right).

6. Conclusion

Flows around a single isolated double-stacked wagon, and multiple wagons with a gap ratio combination $G_f = 9.38W$ and $G_b = 3.23W$, have been simulated and compared with experimental measurements. To this end, the larger objective of this study was to evaluate the capability of the ELES, SAS, URANS and RANS approaches to predict the aerodynamic flow and forces for a double-stacked freight wagon, both in isolation and within a train, by comparing predictions with the wind-tunnel experiments conducted by Li et al. (2017). The Reynolds number in the simulation was $Re_w = 0.3 \times 10^6$ based on the width of the wagon, in agreement with the wind-tunnel experiments. Spatial and temporal resolution studies indicate that the simulations provided well converged predictions.

Table 4
Comparison of CPU time used for various turbulence models for case 2.

Method	Elements	CPU Hours Used	% diff
ELES-4.5W-1.5H	18.5 million	11200	66
SAS-CD	11 million	5600	33
SAS-BCD	11 million	4400	26
URANS	11 million	4000	24
RANS	3 million	170	1

The URANS and RANS models have shown their incapability to correctly predict the flow field for both cases for the rear surface where flow separation occurs. It has been demonstrated that the ELES and SAS approaches provide more accurate results than URANS and RANS, in terms of the pressure drag coefficient, front and base C_p contours, and skin-friction patterns on the top and sides of the wagon. The pressure drag coefficients computed by ELES and SAS were within 1% of the experimental value for the single wagon. In addition, their predictions were only 2% different from wind-tunnel values for the double-stacked freight wagon within a train. The surface pressure distributions and surface flow topologies predicted by ELES and SAS were in a good agreement with the wind tunnel results, both qualitatively and qualitatively. However, there were some differences in the velocity predictions through the recirculation bubbles on the top of the wagon, although the mean reattachment lines were reasonably well predicted. Finally, the computational expense of the each model was provided suggesting RANS may be the most suitable approach for a freight train company if only a relative drag prediction is required.

Acknowledgement

The research described in this paper was supported by both Pacific National Rail and the Australian Research Council's Linkage Project funding scheme, under project number LP13100953. SM would also like to acknowledge partial PhD scholarship funding through this grant.

References

Ahmed, S.R., Ramm, G., Faitin, G., 1984. Some salient features of the time-averaged ground vehicle wake. Technical report. Society of Automotive Engineers, Inc., Warrendale, PA, USA.

Ashton, N., West, A., Lardeau, S., Revell, A., 2016. Assessment of RANS and DES methods for realistic automotive models. Comput. Fluids 128, 1–15.

Davidson L. 2006. Evaluation of the SST-SAS model: channel flow, asymmetric diffuser and axisymmetric hill, in Proceedings of European Conference on Computational Fluid Dynamics: ECCOMAS CFD 2006.

Flynn, D., Hemida, H., Soper, D., Baker, C., 2014. Detached-eddy simulation of the slipstream of an operational freight train. J. Wind Eng. Ind. Aerodyn. 132, 1–12.

Flynn, D., Hemida, H., Baker, C., 2016. On the effect of crosswinds on the slipstream of a freight train and associated effects. J. Wind Eng. Ind. Aerodyn. 156, 14–28.

Frohlich, J., von Terzi, D., 2008. Hybrid LES/RANS methods for simulation of turbulent flows. Prog. Aerosp. Sci. 44 (5), 349–377.

Golovanevskiy, V.A., Chmovzh, V.V., Girka, Y.V., 2012. On the optimal model configuration for aerodynamic modelling of open cargo railway train. J. Wind Eng. Ind. Aerodyn. 107, 131–139.

Hemida, H., Baker, C., 2010. Large-eddy simulation of the flow around a freight wagon subjected to a crosswind. Comput. Fluids 39, 1944–1956.

Li, C., Kost, M., Burton, D., Sheridan, J., Thompson, M.C., 2015. Wind tunnel investigation of a double stacked wagon in free-stream. In: Proceedings of ASME/JSME/KSME 2015 Joint Fluids Engineering Conference. American Society of Mechanical Engineers. V001T16A002.

Li, C., Burton, D., Kost, M., Sheridan, J., Thompson, M.C., 2017. Flow topology of a container train wagon subjected to varying local loading configurations. J. Wind Eng. Ind. Aerodyn. 169, 12–29.

Lienhart, H., Becker, S., 2003. Flow and turbulent structure in the wake of a simplified car model. Society of Automotive Engineers. Technical Paper 2003-01-0656.

Mathey F., Cokljat D., Bertoglio J.P. & Sergent E. 2003. Specification of LES inlet boundary condition using vortex method, in Proceedings of the 4th International Symposium on Turbulence, Heat and Mass Transfer, Antalya, 2003.

Menter, F.R., Egorov, Y., 2010. The scale-adaptive simulation method for unsteady turbulent flow predictions. Part 1: theory and model description. Flow Turbul. Combust. 85, 113–138.

Mirzaei, M., Krajnovic, S., 2016. Numerical study of aerodynamic interactions in a homogeneous multi-vehicle formation. In: Proceedings of the 5th International Conference on Jets, Wakes and Separated Flows (ICJWSF2015). Springer, pp. 289–294.

Osth, J., Krajnovic, S., 2014. A study of the aerodynamics of a generic container freight wagon using large-eddy simulation. J. Fluids Struct. 44, 31–51.

O'Rourke, M.D., Watkins, S., Saunders, J.W., 1990. Aerodynamic resistance and design principles for unit train rail vehicles. end of grant report, ISBN: 0642127425.

Sagaut, P., Deck, S., Terracol, M., 2013. Multi-scale and multi-resolution approaches in turbulence LES, DES and hybrid RANS/LES methods: applications and guidelines, second ed. Imperial College Press.

Schito P., Braghin F., Numerical and experimental investigation on vehicles in platoon, SAE paper 2012-01-0175.

Soper, D., Baker, C., Sterling, M., 2014. Experimental investigation of the slipstream development around a container freight train using a moving model facility. J. Wind Eng. Ind. Aerodyn. 135, 105–117.

Uystepruyst, D., Krajnovic, S., 2013. Les of the flow around several cuboids in a row. Int. J. Heat Fluid Flow 44, 414–424.

Wang, S., Bell, J.R., Burton, D., Herbst, A., Sheridan, J., Thompson, M.C., 2017. The accuracy of different turbulence models (URANS, SAS and DES) for predicting high-speed train slipstream. J. Wind Eng. Ind. Aerodyn. 165, 46–57.